CLM-P288

United Kingdom Atomic Energy Authority
RESEARCH GROUP

Preprint

SPECTROSCOPIC STUDY AND ENERGY BALANCE OF PULSED TOROIDAL DISCHARGES

F E IRONS
W R ELLIS
A A NEWTON

Culham Laboratory
Abingdon Berkshire

1971

CLM-P 288

SPECTROSCOPIC STUDY AND ENERGY BALANCE OF PULSED TOROIDAL DISCHARGES

F E Irons[+], W R Ellis[*] and A A Newton

(To be submitted for publication in Plasma Physics)

A B S T R A C T

Investigations of plasma produced by a pulsed current of 40 kA peak and 20 μs decay time in a quartz torus of major radius 32 cm and minor radius 4 cm in 30 mtorr of hydrogen are described. The electron temperature rose in 1 μs to ~ 4×10^4 K and relaxed by 4 μs to a value of 2×10^4 K for most of the 50 μs duration of the current pulse. Corresponding electron densities were 3×10^{15} cm^{-3} falling to a nearly steady value of 1.5×10^{15} cm^{-3}. At later times the afterglow is followed to 8×10^{13} cm^{-3} at 180 μs.

Dissipation of the toroidal current provides 15 to 20 times the energy required for full ionisation, and temperature equilibrium results from atom thermal conduction loss to the wall. Although these losses can be intrinsic, the observed asymmetries in luminosity and magnetic field show that MHD instability is present which enhances the wall contact.

[+] Now at the School of Physical Sciences, Australian National University, Canberra A.C.T. 2600, Australia

[*] Now at Los Alamos Scientific Laboratory, New Mexico, USA

UKAEA Research Group
Culham Laboratory,
Abingdon,
Berks.

August 1971

1. Introduction

The generation of highly ionised hydrogen in a toroidal vessel by a single current pulse has been studied using several techniques (Ellis and Newton, 1971). Breakdown is produced by induction in a one turn air core transformer with 3.6 kJ capacitive stored energy in the primary at 60 kV giving a peak gas current of 40 kA. At the filling pressures of a few tens of mtorr the breakdown is sensitive to the pressure and to the strength of the steady magnetic field which is applied parallel to the major circumference of the vessel (Malesani et al., 1970). The breakdown lag is comparable to the circuit rise time so that the gas current contains a substantial uni-directional component, hereafter called the "trapped current" (Ellis and Newton, 1971).

This paper presents spectroscopic investigations of the plasma from the start of the current pulse to the afterglow. Radial distributions of electron temperature and density are inferred from space resolved measurements of the line H_α and the continuum at $\lambda = 4961$ Å. These show that the plasma has a density of 1.5×10^{15} cm^{-3} which falls to 8×10^{13} cm^{-3} at 180 μs, with corresponding electron temperatures ranging from 2×10^4 K to 4×10^3 K.

From examination of the energy balance it will be shown that dissipation of the trapped current releases fifteen to twenty times the gas ionisation energy during 50 μs. Since the measured temperature never rises above 4×10^4 K, we conclude that some potent loss mechanism is present. Several energy sinks have been considered. Observations show a weakly ionised region close to the wall and estimates of the electron-atom collision rate and thermal conductivity in this region show that appreciable energy is lost to the wall. Although such regions grow spontaneously as the result of plasma-to-wall contact (Long and Newton, 1971), this process may be enhanced by magnetohydrodynamic instabilities.

2. Apparatus

Plasma is produced in a quartz torus of 32 cm major radius, R, and 4 cm internal minor radius, r_w. The initial gas pressure is 30 mtorr. A quasi steady magnetic field, B_z, of 2 kG uniform to 1% at the tube axis is directed around the major circumference. The discharge is induced with a 2.16 μF, 60 kV capacitor feeding a metal shell surrounding the torus. Following breakdown, a current I_z flows in the gas parallel to B_z, reaching a first peak value of 26 kA in 1 μs and reversing to a second peak of 40 kA by 4 μs (see Fig. 1). It contains a unidirectional component which decays with a 17 μs characteristic time with a damped oscillation superimposed. More details are given elsewhere (Ellis and Newton, 1971). Unless stated, results given below refer to these conditions, which are denoted I. Discharges in a second apparatus with R = 100 cm, r_w = 6 cm in deuterium at 30 mtorr, a B_z of 1.3 or 4.3 kG, which was spatially more uniform, and with a similar current pulse of 30 kA first peak were also investigated (Bodin et al., 1971). These conditions are denoted IIa for 1.3 kG and IIb for 4.3 kG.

Spectroscopic measurements have been made with an Ebert monochromator (resolution 0.25 Å; inverse dispersion 9.0 Å/mm) using a photomultiplier (E.M.I. type 9594QB) and the system was calibrated for absolute intensities using a tungsten lamp. The plasma was viewed through a set of holes in the primary current shell which permitted radial intensity distributions to be measured. Due to surface imperfections and curvature of the quartz, the spatial resolution was limited to ~ 0.8 cm.

3. Theory

In this section the theory required for the interpretation of continuum and line intensities is summarised. The visible continuum contains contributions from both free-free and free-bound transitions and theoretical expressions have been given by Elwert (1954). The intensity can be expressed as

$$I_\lambda(\text{CONT}) = N_e^2 f_\lambda(T_e) \text{ ergs cm}^{-3} \text{ s}^{-1} \text{ sr}^{-1} \text{ Å}^{-1} \quad \ldots (1)$$

where the function $f_\lambda(T_e)$ or $\frac{I_\lambda(CONT)}{N_e^2}$ is shown in Fig. 2, for the wavelength $\lambda = 4961$ Å. This function is only weakly temperature dependent in the range of interest ($4 \times 10^4 - 4 \times 10^3$ K), and the values of N_e derived from measurements of $I_\lambda(CONT)$ incur only a small error due to errors in T_e. The wavelength region around $\lambda = 4961$ Å is free from impurity lines.

The Balmer line intensities are related to N_e and T_e by the Saha-Boltzmann equation, modified by the factor ρ_n to allow for departures from local thermal equilibrium, viz.

$$I_{n2} = \frac{A_{n2}\, h\nu}{4\pi} \quad \frac{\rho_n N_e^2}{2(2\pi m k T_e)^{3/2}} \quad \frac{\omega(0,n)}{\omega(1,1)} \quad \exp\left(\frac{\chi_n}{kT_e}\right) \text{ ergs cm}^{-3}\text{ s}^{-1}\text{sr}^{-1} \qquad \ldots (2)$$

in the usual notation (e.g. McWhirter, 1965). Fig. 2 shows I_{32}/N_e^2 (the H_α line) versus T_e. The weak density dependence is due to ρ_3, values of which have been taken from the tables of Bates et al. (1963). The ratio of line to continuum intensity thus provides a sensitive measure of T_e, and is almost independent of density in the range of interest ($0.5 - 2 \times 10^{15}$ cm^{-3}). The line H_α has been chosen in preference to other Balmer lines because of its greater sensitivity to T_e. Substitution of the observed half-widths into the relevant equation of Cooper (1966) shows that this line is optically thin.

4. Experimental Results

4.1 Radial intensity distributions

Distributions of a 9 Å band of continuum emission centred at 4961 Å and H_α line radiation were built up on a shot-to-shot basis, using six discharges at each of twelve positions across the tube. Except for a short time interval between 14-20 μs after the start of the discharge, these spatial profiles were symmetrical and could be inverted to give radial intensity distributions, following the procedure of Larkin (1969).

The distributions of continuum intensity were approximately uniform out to ~ 80% of the tube radius, falling to low values at the wall, at all times except in the first 8 μs when they tended to peak at a radius of 3.5 cm.

The distributions of line intensity (see Fig. 3) show a strong peak at large radii during the first 50 μs with a smaller peak occuring on axis at early times. These profiles are smoothed due to limited spatial resolution and uncertainties in the measurements at large radii. From 50 to 100 μs the intensity on axis increases, becoming comparable with that near the wall, and after 100 μs the emission is approximately uniform. Between 14 and 20 μs the distributions are asymmetrical with the emission from the upper half of the torus 30% greater for continuum and 200% greater for H_α than that from the lower half.

4.2 Electron temperature and density

The absolute intensities of the continuum were interpreted by means of equation (1) to give $N_e(r)$ and the relative intensities of the line and continuum were interpreted using the curves of Fig. 2 to give $T_e(r)$. Radial distributions are shown in Figs. 4 and 5, where the experimental values have been joined by smooth curves. Figs. 6 and 7 show mean values of N_e and T_e.

At 1 μs the measured electron density exceeds the initial filling density by 50%, which is above the experimental errors. Measurements and estimates of the plasma compression at this time (Ellis and Newton, 1971) show that the local electron density may rise 20% above the filling density which is just outside the measurement errors. Some additional contribution to the continuum may be possible due to non thermal effects and these in turn give rise to corresponding uncertainties in the electron temperatures at this time.

After the initial transient behaviour N_e is approximately uniform with radius at 1.5×10^{15} cm^{-3} for 50 μs, falling near the wall (see Fig. 4). At later times (i.e. during the afterglow) N_e decays with a characteristic time of about 45 μs (see Fig. 6). Initially the temperature rises to a peak of $4 \pm 1 \times 10^4$ K at 3 cm radius in 1 μs and falls by 4 μs to 2×10^4 K. T_e remains at about this value for 50 μs (see Fig. 5) before decreasing in the afterglow.

4.3 Measurements using line emission only

Other measurements of N_e have been made from Stark broadening and of T_e from the Balmer decrement, the plasma being viewed along a minor diameter. Mean values of N_e and T_e have been obtained for the line-emitting region of plasma up to 180 μs, after which time the lines cannot be detected.

The Stark broadening of H_β and H_δ was measured from line profiles built up from about 50 discharges. A family of theoretical Stark profiles (Kepple and Griem 1969), folded with instrumental and Doppler profiles, were matched against each experimental profile, and a density was assigned, with an uncertainty of ± 15%. The results are shown in Fig. 6, where it can be seen that the values of N_e determined from the two lines are in good agreement, except for the period 4 to 40 μs when there are steep density and temperature gradients near the wall which cause a small separation in the regions of H_β and H_δ emission. This density rises from 3×10^{14} cm^{-3} to a maximum of $\sim 1.4 \times 10^{15}$ cm^{-3} by 14 μs, and then falls to join smoothly at 8×10^{13} cm^{-3} to 2 mm microwave interferometric measurements.

To determine the electron temperature from the Balmer decrement, mean values of the intensities of $H_{\alpha,\beta,\gamma,\delta,\varepsilon}$ were measured, using eight discharges for each line, correcting for the continuum, and interpreting by the standard method (see e.g. Pearce 1961), taking into consideration non-unity values of ρ_3 and ρ_4. Fig. 7 shows that the temperatures cover a range of 2000-7000 K where the method is sensitive, and the uncertainty is ± 15%.

The above measurements, based only on line radiation, relate to the regions where line emission from the plasma is strong. At times greater than 100 μs the line emission is uniform with radius and the measured values of N_e and T_e then represent average values which match with the other measurements. At earlier times the line measurements relate to the regions of strong line emission which are near the wall: for completeness these measurements are included in the radial profiles in Figs. 4 and 5 where they have been plotted at the radii

corresponding to peak line emission. They are in good agreement with the other measurements at these radii.

4.4 Depth of the line-emitting region

From equation (2) the absolute volume emission of the lines was calculated, using the values of N_e and T_e derived from line intensities (Section 4.3). The observed absolute surface emission was then used to estimate the depth of the line-emitting region of plasma. The result, which is the average of values found using the intensities of all five lines, is shown in Fig. 8. There is agreement with the data of Fig. 3, which shows an initially thin line-emitting region, broadening with time to occupy the full tube radius by about 80 μs. At times before 30 μs the values of depth in Fig. 8 are smaller than the spatial resolution of the data in Fig. 3 ($\approx$ 0.8 cm) and give the more accurate measurement of the depth of the line-emitting region at these times.

4.5 Other results and summary

Less detailed observations on the second device (II) (Bodin et al. 1971), with a somewhat lower axial current density, show similar behaviour, and all results are summarised in Table I. For II the electron density and temperature in the body of the plasma were measured, respectively, from the absolute intensity of the continuum at λ = 5100 Å and from the intensity ratio of two equal bandwidths of continuum at λ = 5100 and 3440 Å, the plasma being viewed across a diameter. The initial peak electron temperatures were significantly higher in II but relaxed to a lower steady value during the remainder of the current pulse. Electron temperatures in the cold outer region were comparable in I and II. Electron densities in the same region were a factor $\sim$ 5 smaller in II. In II the electron densities were found to be identical when measured viewing in the plane of, and perpendicular to, the toroidal (non equilibrium) drift. At the higher value of B_z, i.e. IIb, the initial values of T_e in the body of the plasma and in the outer layer were somewhat smaller than in IIa. Values for the afterglow (in Table I) of IIa and IIb are not quoted because the

behaviour is partly determined by the decay of B_z which has an e-folding time of < 1 msec.

Additional measurements in IIa and IIb of the perturbed radial magnetic field showed fluctuations after 1 to 2 μs characteristic of MHD instabilities.

5. Discussion

5.1 Recombination

Line radiation is emitted preferentially from regions of low temperature where there is negligible ionisation and rapid recombination. Thus the Stark measurement of N_e and the Balmer decrement measurement of T_e relate to that part of the plasma which is recombining. Experimental values of the coefficient γ (defined by $\gamma = -\frac{1}{N_e^2}\frac{dN_e}{dt}$) derived from Stark densities are shown in Fig. 9, together with theoretical values of the recombination coefficient α interpolated from the published tables of Bates et al. (1962), using Stark densities and Balmer decrement temperatures, for plasmas optically thin and thick to lines of the Lyman series. Up to 40 μs the experimental values of γ are much smaller than the theoretical values of α. The densities during this time may represent not the history of an isolated volume of the plasma but the densities of shells of plasma which become successively line-emitting, either (i) at different radii as a result of the plasma cooling from the outside (on this model the radius of the hot region would decrease by ~ 1 cm in 40 μs), or (ii) in a region near the wall as a result of an outward motion due to convection or hydromagnetic instability. The radial profile measurements lack sufficient spatial resolution to distinguish between these two explanations.

From 40 to 70 μs the plasma on axis cools, and the temperature and line emission become more uniform across the tube and the experimental values of γ come into agreement with the theoretical values of α. After 100 μs the Stark derived values of N_e, γ and the Balmer decrement values of T_e are representative of the plasma as a whole, which decays uniformly by recombination. Behaviour in this period agrees well with observations of similar plasmas

(e.g. Newton and Sexton, 1968 and 1969, Parkinson, 1969).

In the body of the plasma up to 40 μs the electron temperature and density are such that recombination is not expected and any atoms present would be ionised within ~ 10 μs. The fact that the electron density is observed not to increase during this period indicates that either there are no neutrals in the body of the plasma or there is an outward flow. Integration over the whole volume of line-emitting plasma up to 40 μs using the theoretical recombination coefficient shows that the total number of ions recombined is $0.8 \pm 0.4 \times 10^{19}$. This number plus the number of ions still present in the plasma at 40 μs ($0.9 \pm 0.3 \times 10^{19}$) account for most of the atoms initially present (2.1×10^{19}).

5.2 Energy balance

A significant energy is stored inductively in the trapped current, which is dissipated in the plasma, and estimates of the joule heating show that in the first 50 μs the plasma receives about 15 to 20 times more energy than is required for full ionisation. Since the plasma is not significantly heated beyond 4×10^4 K, temperature equilibrium must be maintained by one or more loss processes. Estimates of the radiative loss using published data (Bates and Kingston, 1963) show this to be small. Measurements of the impurity content indicate a trace of carbon and of oxygen and the intensity of the line OIII 3265 Å doubled when 0.01% of oxygen was added. Estimates indicate that the energy lost by impurity radiation is negligible.

The energy loss can be accounted for by atom thermal conduction in the outer regions of the plasma and estimates based on the observed densities and temperatures show that a sink comparable to the joule heating can be expected. Atom thermal conduction has previously been found to be important in dense plasma afterglows where the electron-atom energy equipartition rate of $10^{-10}\ \phi(T_e)\ (T_e - T_a)\ n_e n_a$ eV cm^{-3} sec^{-1} ($\phi(T_e) \sim 2$ in the range of interest) is sufficient to ensure comparable temperatures for these species (e.g. Bates and Kingston, 1964,

Irons and Millar, 1965, Cooper and Kunkel, 1966, Newton and Sexton, 1968 and Parkinson, 1969). The atom thermal conduction loss, L_a, can be estimated assuming $T_e = T_a$ as

$$L_a = \kappa_{ao} T_a \frac{\Delta T_a}{\Delta r} \cdot 4\pi^2 r_w R$$

where $\kappa_{ao} = 40$ erg sec^{-1} cm^{-1} K^{-2} and $T_a, \Delta T_a$ and Δ_r are equated to the temperature of, the temperature drop across, and the depth of, the line emitting region.

Power balance for the plasma is shown in Fig. 10. Here calculations are shown of the power dissipated by the current, of the power lost by radiation and by atom thermal conduction, and also of the plasma power loss (ionisation and thermal). The dissipated power, $I_p^2 R_p$ is calculated using values of plasma resistance, R_p, derived from the period and damping of the current waveform (Ellis and Newton, 1971). The radiated power is calculated for the observed values of N_e and T_e from the tables of Bates and Kingston (1963), and is shown for the limiting cases of plasma optically thin and thick to lines of the Lyman series.

After ~ 70 μs the ionisation energy released by the recombining plasma can be accounted for by radiation alone, if optically thin conditions are assumed.

The presence of a neutral atom layer near the wall may be an intrinsic property of the plasma or may be due to toroidal non-equilibrium or an MHD instability in its non linear regime. Numerical investigations of the decay of a highly ionised plasma in the absence of magnetic field (Long and Newton, 1971) with initial uniform $T_e = 1.6 \times 10^4$ K and $N_e = 10^{15}$ cm^{-3} show the establishment of a neutral layer ~ 0.5 cm thick with $> 10^{16}$ atoms cm^{-3} in a 4 cm radius tube in 10 μs. Under these conditions the electron neutral collision frequency is sufficient for the B_z magnetic field to have little effect on transport processes.

Measurements on IIa show that MHD instability is dominant with the expected growth rate $\sim 2I_z/r_w^2 \sqrt{4\pi m_i N_e} \sim 10^6$ sec^{-1} (Robinson, 1971). Toroidal drift effects were not seen. It is concluded that high T_e are permitted only in the

first 1-2 μs until an MHD instability grows causing rapid plasma-wall contact through the accumulation of a region of neutral atoms. Continuing instability is expected to transport plasma towards the wall and sustain the electron density and radiance in the outer layer (see Section 5.1).

Electron temperatures in the body of the plasma when wall contact has been established can be predicted dimensionally by assuming that the joule heating (with plasma resistivity of the form $\eta_o/T_e^{3/2}$) in the outer region is lost to atom thermal conduction. If it is also assumed that $T_e \sim T_a$ then

$$T_e \sim \left[\frac{\eta_o I_z^2}{2\pi^2 r_w^2 \kappa_{ao}} \frac{\Delta r}{r_w} \right]^{2/7}$$

which is consistent with observations with $\Delta r/r_w \sim 0.1$ for both experiments.

6. Conclusions

From spectroscopic measurements on pulsed toroidal discharges it is found that the electron temperature rises rapidly in the first microsecond to $3 \times 10^4 - 9 \times 10^4$ K and there is a high level of ionisation (i.e. $N_e \sim 2 \times 10^{15} cm^{-3}$ The temperature then relaxes in a few microseconds to an approximately steady value of $1.5 \times 10^4 - 2.0 \times 10^4$ K for the 50 μs duration of the current pulse. The electron density behaves in a similar manner falling to an average value corresponding to 35 - 70% of the initial atom filling density. At later times, when the current has decayed, an afterglow with a characteristic time of 45 μs is observed with the electron density, as measured by Stark broadening and microwave interferometry, falling to 8×10^{13} cm^{-3} at 180 μs.

The loss rate of electrons agrees with that expected from three body recombination in the afterglow. However, during the current pulse there is a thin layer near the wall which remains radiant for a much longer time than would be expected for recombination within an isolated volume. This behaviour can be explained by a continuing flow of plasma into the wall region and contrasts with the early afterglow where the plasma becomes uniformly radiant.

Examination of the energy balance shows that the dissipation of inductive

energy associated with the "trapped current" can be quickly passed by electrons, to atoms and then to the wall by atom thermal transport. The latter mechanism, which is operative in certain types of afterglow, is expected in this experiment, and MHD instability, driven by the trapped current, enhances the effect.

Acknowledgements

It is a pleasure to acknowledge discussions with H.A.B. Bodin and D.C. Robinson and also L. Firth and M. Holloway for assistance with the experiment.

Table I. Summary of characteristics and observations of toroidal pulsed discharges

EXPT.	I	IIa	IIb
Gas and filling pressure	30 mtorr H_2	30 mtorr D_2	
Major Radius R cm	32	100	
Minor Radius r_w cm	4	6	
Peak Current I_z kA	40	30	
Axial magnetic field kG	2.0	1.3	4.3
Electron temperatures K			
(a) Initial peak	40,000	90,000	60,000
(b) Typical, in body of plasma during current pulse	20,000	15,000	13,000
(c) Outer layer, early times	1,500 @ 2 μs	1,000 @ 3 μs	1,300 @ 3μs
(d) Outer layer, peak	7,500 @ 50 μs	7,500 @ 25 μs	5,500 @ 45 μs
(e) Afterglow	4,000 @ 180 μs	*	*
Electron densities cm^{-3}			
(a) Initial peak	3.1×10^{15} @ 1 μs	3.0×10^{15} @ 1 μs	3.0×10^{15} @ 1 μs
(b) Typical, in body of plasma during current pulse	1.5×10^{15}	0.8×10^{15}	1.0×10^{15}
(c) Outer layer, early times	$3 \pm 1 \times 10^{14}$ @ 2 μs	6×10^{13} @ 2 μs	5×10^{13} @ 3 μs
(d) Outer layer, peak	1.4×10^{15} @ 20 μs	3.5×10^{14} @ 40 μs	5.5×10^{14} @ 30μs
(e) Afterglow	8×10^{13} @ 180 μs	*	*
Afterglow density decay time	45 μs	*	*

References

Bates, D.R. and Kingston, A.E., 1963 Planetary and Space Science 11, 1-22.

Bates, D.R. and Kingston, A.E., 1964 Proc. Roy. Soc. A, 279, 10.

Bates, D.R., Kingston, A.E. and McWhirter, R.W.P., 1962 Proc. Roy. Soc. A, 267, 297 and 270, 155.

Bodin, H.A.B. and Newton, A.A., 1969, Phys. Fluids, 12, 2175.

Bodin, H.A.B. et al., IAEA Conference on Plasma Physics and Controlled Fusion, Madison, 1971. Paper CN-28/B-5.

Cooper, J., 1966, Reports on Progress in Physics, 29, 35-130.

Cooper, W.S. and Kunkel, W.B., 1965 Phys. Rev. 138A, 1022-7.

Ellis, W.R. and Newton, A.A., to be published.

Elwert, G., 1954, Z. Naturf. 9A, 637-53.

Hain, K., Hain, G., Roberts, K.V., Roberts, S.J. and Koppendorfer, W., 1960, Z. Naturforsch 15A, 1039.

Irons, F.E. and Millar, D.D., 1965, Aust. J. Phys. 18, 23-39.

Kepple, P. and Griem, H.R., 1969, University of Maryland Report No. 831.

Long, J.W. and Newton, A.A. 1971, Tenth Conference on Ionisation Phenomena in Gases, Oxford.

Larkin, F.M., 1969, Tidskrift Informations Behandling 11, 1-22 (also CLM-P179).

Malesani, G., Ellis, W.R. and Newton, A.A., 1970. Proceedings of the Fourth European Conference on Controlled Fusion and Plasma Physics, Rome. p.42.

McWhirter, R.W.P., 1965, "Plasma Diagnostic Techniques", Ed. Huddlestone, R.H. and Leonard, S.L. (New York: Academic Press) Chapter 5.

Newton, A.A. and Sexton, M.C., 1968, J. Phys. B 1, 669-79.

Newton, A.A. and Sexton, M.C., 1969, J. Phys. B 2, 1069-74.

Parkinson, G.J., 1969, Thesis, University of London.

Pearce, W.J., 1961, "Optical Spectrometric Measurements of High Temperatures", Ed. Dickerman, P.J. (University of Chicago Press) pp. 125-169.

Robinson, D.C., 1971, Culham Laboratory Preprint, CLM-P 247.

Spitzer, L., 1962, "Physics of Fully Ionized Gases", Interscience Publishers Ltd. (New York and London).

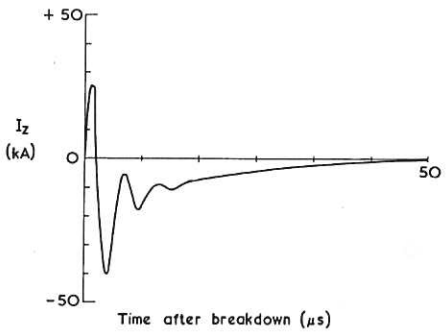

Fig. 1 Plasma current, I_z, as a function of time.

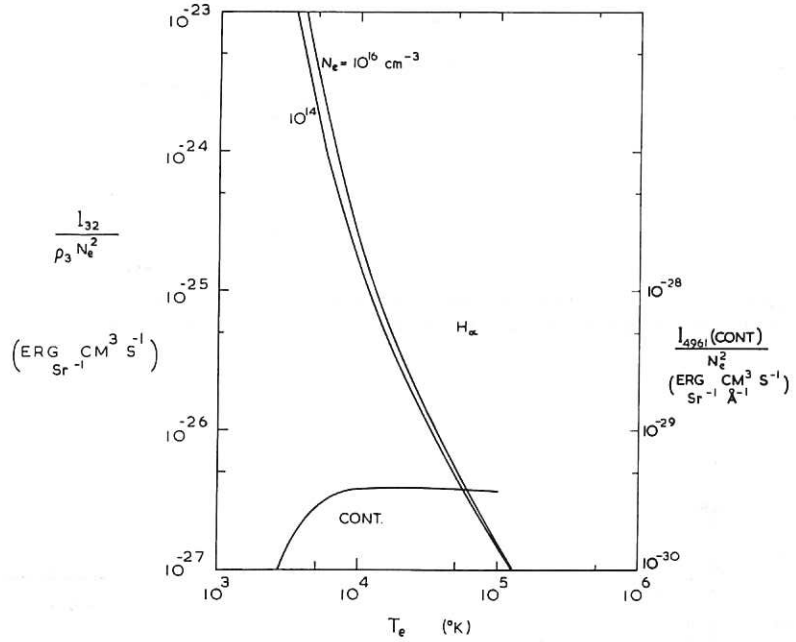

Fig. 2 Graph showing the temperature dependence of the intensity of the line H_α and of the continuum at λ = 4961 Å.

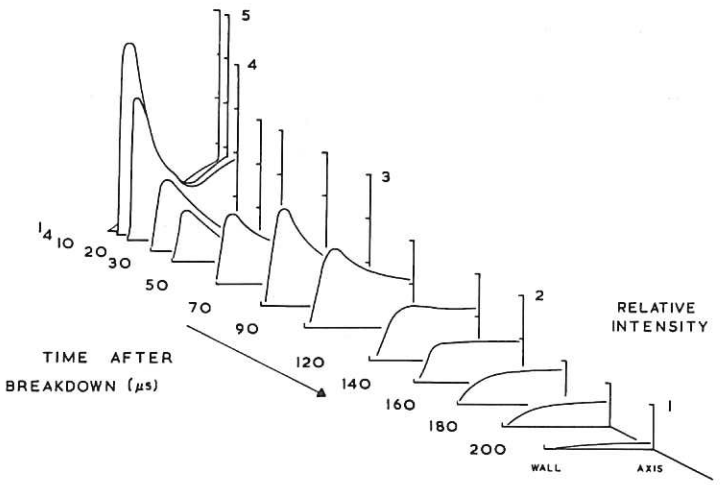

Fig. 3 Radial intensity profiles of H_α.

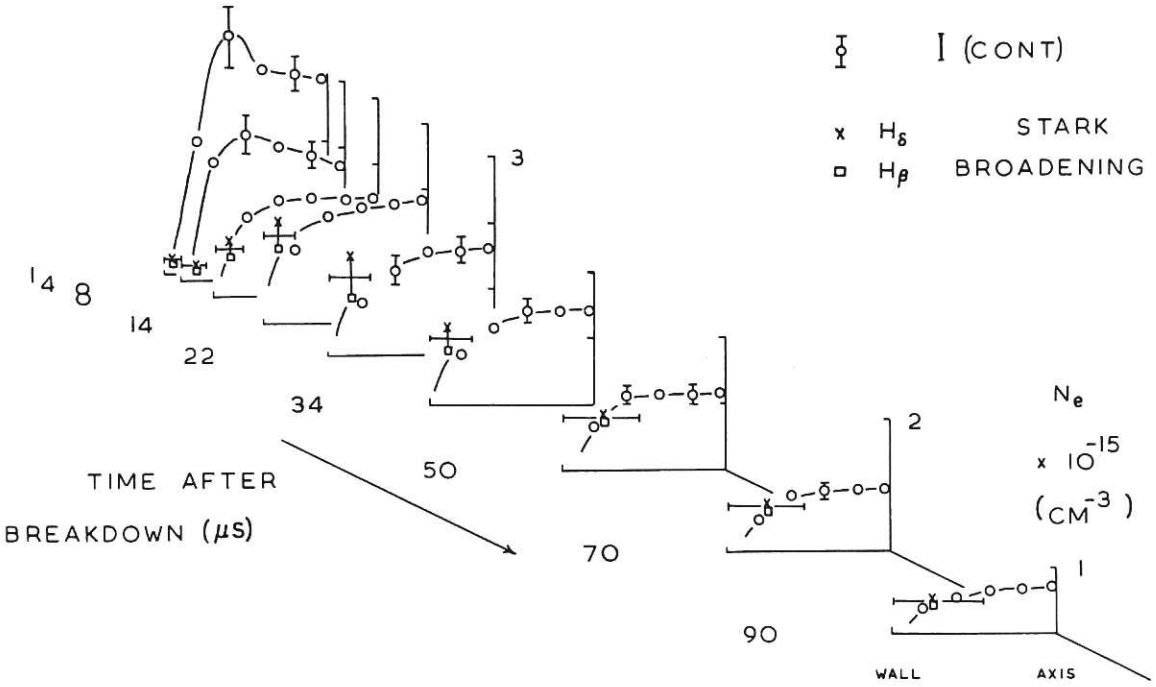

Fig. 4 Radial profiles of electron density from the absolute continuum intensity, with some points from diametrical observations of Stark broadening.

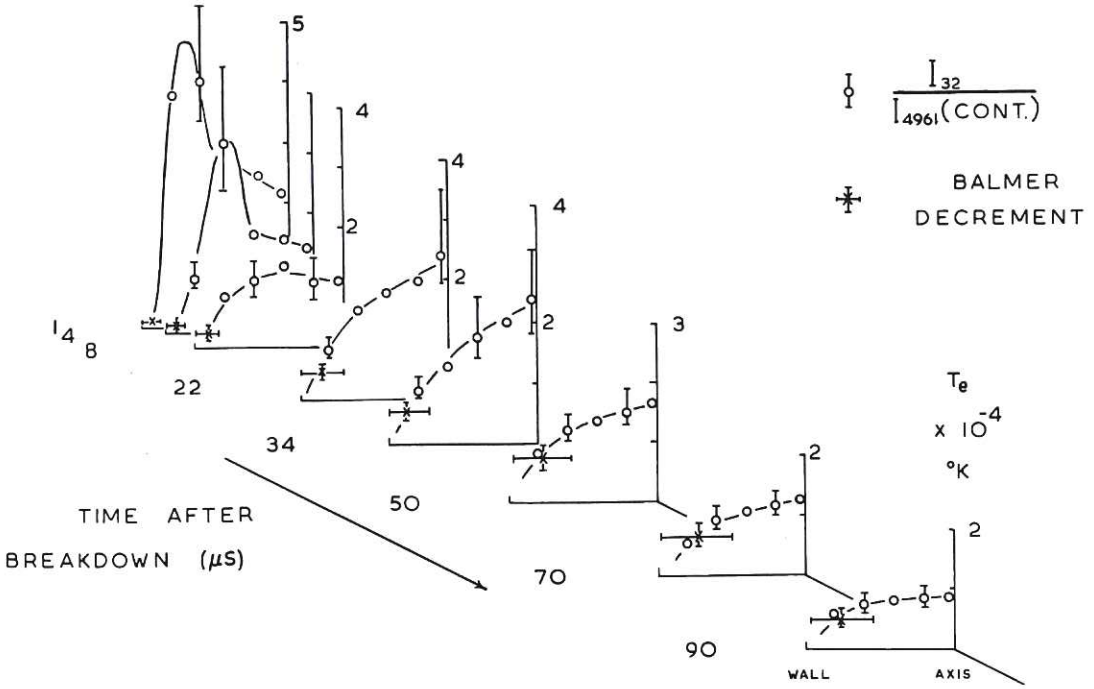

Fig. 5 Radial profiles of electron temperature from the ratio of the line to continuum intensity, with some points from diametrical observations of the Balmer decrement.

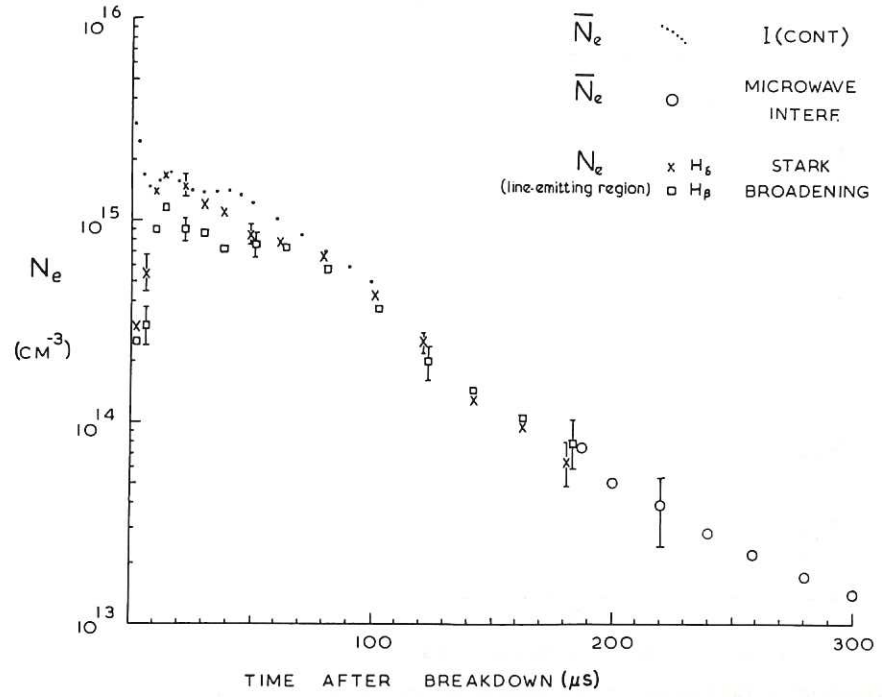

Fig. 6 The time history of the electron density from the continuum intensity averaged over the tube diameter, and of the density of the line-emitting region of plasma from diametrical observations of Stark broadening.

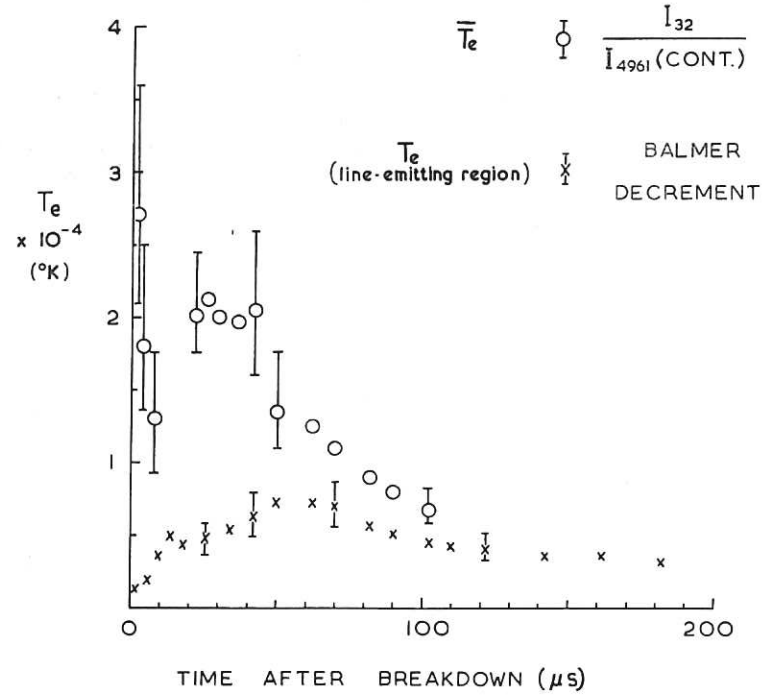

Fig. 7 The time history of the electron temperature from the ratio of line to continuum intensity averaged over the tube diameter, and of the temperature of the line-emitting region of plasma from diametrical observations of the Balmer decrement.

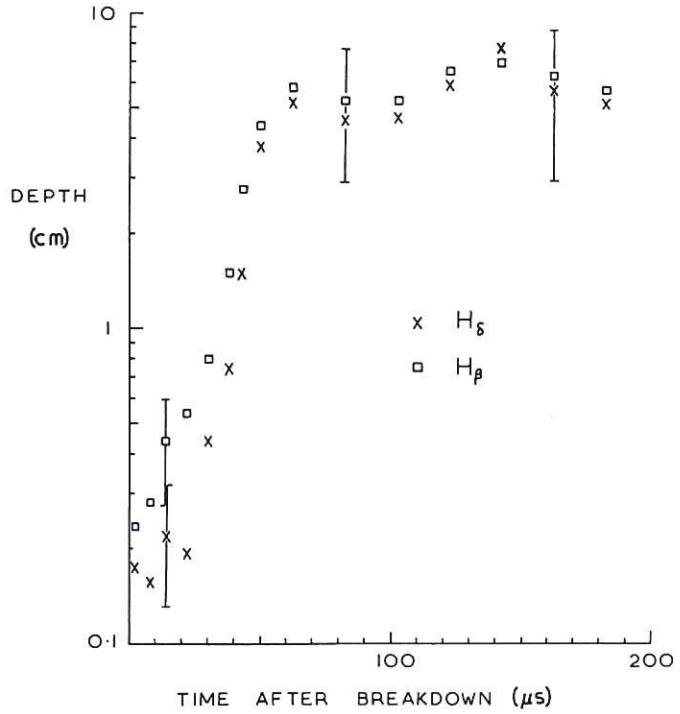

Fig. 8 The depth of the line-emitting region of plasma as derived from line intensities, for Stark densities from both H_β and H_δ.

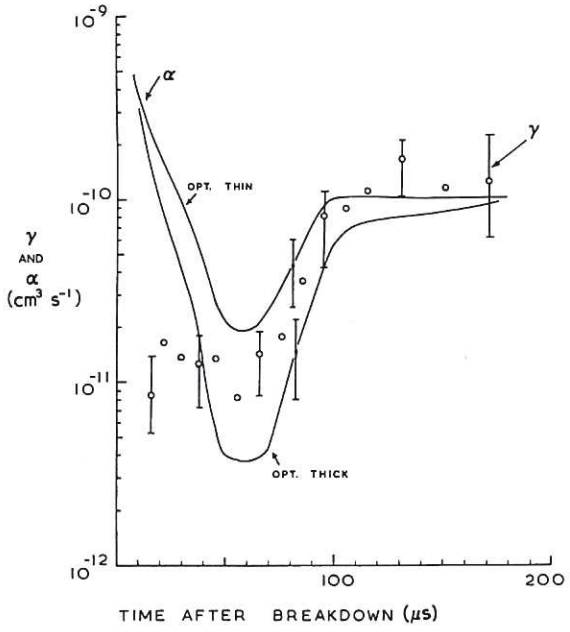

Fig. 9 Graph showing the experimental values of γ (defined by $\gamma = -\frac{1}{N_e^2}\frac{dN_e}{dt}$), and the theoretical values of the recombination coefficient α.

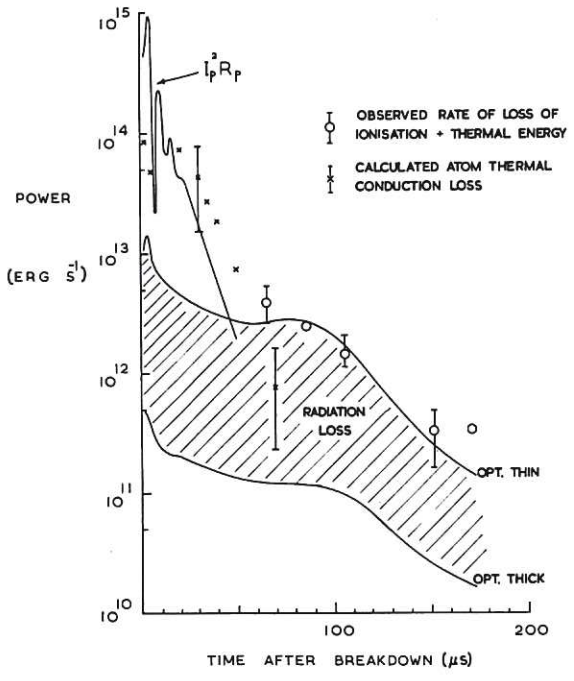

Fig. 10 Graph showing the power balance, initially between the power input $I_p^2R_p$ and the atom thermal conduction loss, and ultimately between the observed rate of loss of ionization plus thermal energy and the radiation loss.